


# Improved photovoltaic performance of monocrystalline silicon solar cell through luminescent down-converting $\text{Gd}_2\text{O}_2\text{S:Tb}^{3+}$ phosphor

Fanchao Meng<sup>1</sup>  | Zahir Dehouche<sup>1</sup> | Terry G. Ireland<sup>2</sup> | George R. Fern<sup>2</sup>

<sup>1</sup>College of Engineering, Design and Physical Sciences, Brunel University London, Uxbridge, UK

<sup>2</sup>Department of Chemical and Materials Engineering, Brunel University London, Uxbridge, UK

## Correspondence

Fanchao Meng, College of Engineering, Design and Physical Sciences, Brunel University London, Uxbridge UB8 3PH, UK.  
Email: fanchao.meng@brunel.ac.uk

## Abstract

This work reports on efforts to enhance the photovoltaic performance of standard p-type monocrystalline silicon solar cell (mono-Si) through the application of ultraviolet spectral down-converting phosphors. Terbium-doped gadolinium oxysulfide phosphor and undoped-gadolinium oxysulfide precursor powders were prepared by a controlled hydrothermal decomposition of a urea homogeneous precipitation method. The resulting rare-earth element hydroxycarbonate precursor powders were then converted to the oxysulfide by annealing at 900°C in a sulfur atmosphere. The as-prepared phosphors were encapsulated in ethylene vinyl acetate co-polymer resin and applied on the textured surface of solar cell using rotary screen printing. Comparative results from X-ray powder diffraction, field emission scanning electron microscopy, scanning transmission electron microscopy, and photoluminescence spectroscopy studies on the microstructure and luminescent properties of the materials are reported. We also compared the optical reflectance and external quantum efficiency response of the cells with and without a luminescent phosphor layer. The results obtained on the terbium-doped gadolinium oxysulfide phosphor show clearly that the down-conversion effect induced by the terbium dopant play a crucial role in enhancing the photovoltaic cells' performance. Under an empirical one-sun illumination, the modified cells showed an optimum enhancement of 3.6% (from 16.43% to 17.02%) in conversion efficiency relative to bare cells. In the concentration range of 1 to 2.5 mg/mL, EVA/ $\text{Gd}_2\text{O}_2\text{S}$  (blank) composites also improve electrical efficiency, but not as much as EVA/ $\text{Gd}_2\text{O}_2\text{S:Tb}^{3+}$  composites.

## KEYWORDS

down-conversion, ethylene vinyl acetate,  $\text{Gd}_2\text{O}_2\text{S:Tb}^{3+}$ , rotary screen printing, silicon solar cells

**Nomenclature:**  $d_{hkl}$ , Inter-planer spacing;  $E_g$ , Band gap energy; FF, Fill factor;  $hkl$ , Miller indices;  $J_{sc}$ , Short-circuit current density;  $P_{max}$ , Power at maximum power point;  $V_{oc}$ , Open-circuit voltage; wt%, Weight ratio;  $\eta$ , Efficiency;  $\theta$ , Bragg angle

**Abbreviations:** ARCs, anti-reflection coatings; ARC, anti-reflection coating; CIE, International Commission on Illumination; CL, cathodoluminescence; c-Si, crystalline silicon; DC, down-conversion; DI, deionized; EDS, energy dispersive X-ray spectroscopy; EQE, external quantum efficiency; EVA, ethylene vinyl acetate; FE-SEM, field emission-scanning electron microscope; HAADF, high angle annular dark field; IR, infrared; JCPDS, joint committee powder diffraction standards; LDS, luminescent down-shifting; mono-Si, monocrystalline silicon; NIST, national institute of standard and technology; J-V, current density-voltage; PCE, power conversion efficiency; PL, photoluminescence; PLE, photoluminescence excitation; PV, photovoltaic; QY, quantum yield; RI, refractive index; SRM, standard reference material; STEM, scanning transmission electron microscope; UV, ultraviolet; UV-Vis, ultraviolet-visible; XRPD, X-ray powder diffraction

This is an open access article under the terms of the Creative Commons Attribution License, which permits use, distribution and reproduction in any medium, provided the original work is properly cited.

© 2019 The Authors. *Progress in Photovoltaics: Research and Applications* Published by John Wiley & Sons Ltd.

## 1 | INTRODUCTION

The gradual increase in energy consumption and the approaching depletion of fossil fuels have initiated the search for clean and sustainable alternative energy sources. Photovoltaic (PV) cells can be used for the direct generation of electricity from solar radiation, with nearly zero-emission of greenhouse gases. Currently, the crystalline silicon (c-Si)-based solar cells are still dominating the global solar PV market because of their abundance, stability, and non-toxicity.<sup>1,2</sup> However, the conversion efficiency of PV cells is constrained by the spectral mismatch losses, non-radiative recombination and strong thermalisation of charge carriers. Generally, the c-Si solar cells are only able to absorb photons within a limited portion of solar spectrum, with ultraviolet (UV)-blue and most of the infrared (IR) region of light untapped.<sup>3</sup> According to the literature, around 47% of energy conversion is lost as lattice thermalisation, which is caused by the incident photons having energy above the band gap ( $E_g = 1.12$  eV). As a result, the maximum theoretical conversion efficiency for a single-junction c-Si solar cell with energy gap of 1.1 eV is limited to 30%.<sup>4,5</sup> Reducing these losses in c-Si solar cells may be achievable through spectrum modification by employing down-converting phosphors.<sup>6-9</sup> In a down-conversion (DC) process, a high-energy incident photon is absorbed by the DC phosphors and re-emitted as two or more lower energy photons at wavelengths where the silicon solar cells exhibit a strong spectral response.<sup>10,11</sup> A number of researchers have shown that there is significant enhancement in conversion efficiency of solar PV devices by integrating a down-converting or luminescent down-shifting (LDS) layer on the top surface of c-Si solar cells.<sup>12-19</sup>

In recent years, rare-earth element doped-oxysulfides have been extensively investigated and studied because of their efficient performance as luminescent materials. Moreover, their high-conversion efficiency from X-ray wavelengths to visible light, low toxicity, high radiation stability, and easy preparation, which has seen their use in a wide range of applications such as emissive display devices,<sup>20</sup> optical temperature sensors,<sup>21</sup> oxygen storage,<sup>22</sup> X-ray detectors and scintillators.<sup>23</sup> Terbium-doped gadolinium oxysulfide ( $\text{Gd}_2\text{O}_2\text{S:Tb}^{3+}$ ) is reported as the most commonly used phosphor in commercial X-ray intensifying screens. The high density ( $7.34$  g/cm<sup>3</sup>) and wide band gap (4.6-4.8 eV) enable it to effectively trap X-ray photons.<sup>24</sup> The intense green emission of the  $\text{Gd}_2\text{O}_2\text{S:Tb}^{3+}$  phosphor under UV excitation implies its great potential of being used as an efficient spectral converter in an attempt to reduce the spectral mismatch losses while improving the overall light absorption in silicon solar cell.<sup>25,26</sup> The reason that a submicron  $\text{Gd}_2\text{O}_2\text{S:Tb}^{3+}$  phosphor was chosen in place of a commercially available sample was two fold. Firstly, because of the surface texture of the mono-Si solar cell, commercial  $\text{Gd}_2\text{O}_2\text{S:Tb}^{3+}$  phosphor particles with large grain size (average size around  $3.5$   $\mu\text{m}$ ) would not form a close-packed thin phosphor layer; instead, they would reflect some of the incident light and shade the cell because they are larger than the width and depth profile of the textured structures. Secondly, from our previous work with soft X-ray detectors using submicron  $\text{Gd}_2\text{O}_2\text{S:Pr}^{3+}$  phosphor particles to form a thin phosphor layer, it was found that they gave a

higher detection efficiency than a much larger commercial  $\text{Gd}_2\text{O}_2\text{S:Pr}^{3+}$  sample. The higher detection efficiency of the smaller  $\text{Gd}_2\text{O}_2\text{S:Pr}^{3+}$  particles was because of their ability to form a thin close-packed layer with very few "pinholes," thereby capturing more X-rays.<sup>27</sup> In the present work, submicron-sized  $\text{Gd}_2\text{O}_2\text{S:Tb}^{3+}$  phosphor precursor powders were prepared by a urea hydrothermal homogeneous-precipitation method.<sup>28,29</sup> In addition, to encapsulate the phosphor particles on the textured surface of monocrystalline silicon (mono-Si) solar cell, ethylene vinyl acetate (EVA), with excellent optical properties, good thermal stability, and strong adhesion, was selected as the matrix and binder.<sup>30</sup> Hence, we believe that such a luminescent-composite layer could compensate for the low spectral response of silicon solar cell at the UV-blue wavelengths, thereby improving the conversion efficiency.

In this study, we demonstrated a low-cost effective luminescent layer comprising of an EVA/ $\text{Gd}_2\text{O}_2\text{S:Tb}^{3+}$  mixture on the textured surface of commercial single-junction mono-Si solar cell through rotary screen printing. In addition to investigating the morphological and luminescent properties of the  $\text{Gd}_2\text{O}_2\text{S:Tb}^{3+}$  particles, the PV current density-voltage ( $J$ - $V$ ) characteristics, optical reflectance, absorbance, and external quantum efficiency (EQE) response of the solar cell before and after coating were also obtained, in order to compare the cells' PV performance and examine the effectiveness of Tb-doped phosphors.

## 2 | EXPERIMENTAL METHODS

### 2.1 | Materials

The following chemicals were used in this work: gadolinium oxide ( $\text{Gd}_2\text{O}_3$ ) (Ampere Industries, France, 99.99%), terbium oxide ( $\text{Tb}_4\text{O}_7$ ) (Neo materials, UK, 99.99%), nitric acid ( $\text{HNO}_3$ ) (Fisher Scientific, UK, more than 68%), Sulfur (S) (Sigma Aldrich, UK, 99.9%), sodium carbonate ( $\text{Na}_2\text{CO}_3$ ) (Sigma Aldrich, UK, 99.9%), p-xylene (Alfa Aesar, UK, 99%), and ethylene vinyl acetate (EVA) (Elvax 150, DuPont, USA). All chemicals were used as received without further purification.

The solar cells used in this work were commercial p-type mono-Si solar cell (T6S-3A, Motech Industries, Taiwan) prestructured with dark silicon nitride ( $\text{SiN}_x$ ), anti-reflection coatings (ARCs) on the front-textured surface. The  $\text{SiN}_x$  layers were deposited by low pressure plasma-enhanced chemical vapour deposition with an average thickness of approximately 80 nm.

### 2.2 | Synthesis of $\text{Gd}_2\text{O}_2\text{S:Tb}^{3+}$ phosphor

The  $\text{Tb}^{3+}$ -activated  $\text{Gd}_2\text{O}_2\text{S}$  phosphor particles were synthesized through a two-step method: the first step was the preparation of  $\text{Tb}^{3+}$ -doped gadolinium hydroxycarbonate precursor ( $\text{Gd}(\text{OH})\text{CO}_3:\text{Tb}^{3+}$ ) via a urea-based hydrothermal homogeneous precipitation method with minor modifications.<sup>28,29,31</sup> The second step was the sulfuration of the  $\text{Gd}(\text{OH})\text{CO}_3:\text{Tb}^{3+}$ . In order to obtain the highest luminance in the  $\text{Gd}_2\text{O}_2\text{S:Tb}^{3+}$  phosphor samples, the ratio of  $\text{Tb}^{3+}$

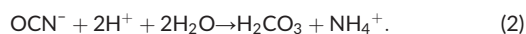
ions was set to 2 mol% in respect with that of  $Gd^{3+}$  molar concentration.<sup>26</sup> Gadolinium nitrate ( $Gd(NO_3)_3$ ) (0.25 M) and terbium nitrate ( $Tb(NO_3)_3$ ) (0.25 M) stock solutions were prepared by respectively dissolving  $Gd_2O_3$  and  $Tb_4O_7$  in dilute nitric acid until the solution reached pH between 1 and 3.

For the preparation of  $Tb^{3+}$ -doped  $Gd(OH)CO_3$  precursor powders,  $Gd(NO_3)_3$  (0.25 M, 50 mL) and  $Tb(NO_3)_3$  (0.25 M, 1 mL) solutions were mixed with deionized (DI) water (900 mL in a beaker). The solution was then heated until boiling, followed by the addition of urea (30 g). The solution was boiled until turbidity was observed at which point the solution was aged for 1 hour at the same temperature. The precipitates were then filtered at the pump while still hot, followed by washing twice with DI water (100 mL) and then dried in an oven at 100°C overnight. For sulfuration of the precursor powders, the as-prepared  $Gd(OH)CO_3:Tb^{3+}$  dry powder was thoroughly mixed with  $Na_2CO_3$  and S, compacted into an alumina crucible, and then covered with a mixed top layer composed of  $Gd_2O_3$ ,  $Na_2CO_3$  and S, in which the molar ratio of the precursor/ $Gd_2O_3$ / $Na_2CO_3$ /S is 1/1/1.5/2. A lid was then placed on the crucible and annealed at 900°C for 1 hour. After annealing, the top layer was discarded and the bottom layer was then washed in boiled DI water (50 mL) for 15 minutes before filtration. The obtained precipitates were dried again at 100°C to yield white soft powders. The undoped- $Gd_2O_2S$  particles were prepared in the same route without adding of Tb dopant. The chemical reactions during the fabrication process are described by the follow equations<sup>24</sup>:

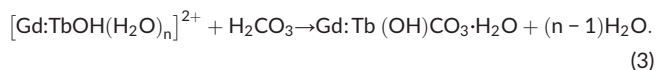
Hydrothermal decomposition of urea (rate 4% per hour at approximately 100°C) supplying reactants in a controlled manner,



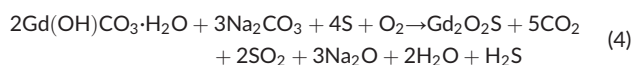
With increasing pH (less than pH 3), the cyanate ion rapidly reacts,



The rare earth element ions are weakly hydrolysed in water, and the subsequent release of hydronium ions promotes urea decomposition, the resulting release of carbonate ions causes precipitation, once the concentration of reactants reaches critical supersaturation,



The resulting ( $Gd(OH)CO_3:Tb^{3+}$ ) precursor powders were converted to the  $Gd_2O_2S:Tb^{3+}$  phosphor by heating at 900°C in a sulfur atmosphere,



## 2.3 | EVA/ $Gd_2O_2S:Tb^{3+}$ layer preparation and integration on the surface of solar cell

For experimental purposes, the cell was previously cut into three equal pieces ( $15.6 \times 5.2$  cm) using a high-power laser machine (TMX90, CTR, UK). The as-prepared  $Gd_2O_2S:Tb^{3+}$  phosphor powder was ready to be used for the layer coating process. In a typical procedure, a stoichiometric amount of phosphor powder was weighed and dispersed in p-xylene using an ultrasonic bath. A series of solutions containing the  $Gd_2O_2S:Tb^{3+}$ /p-xylene with 1.0, 1.5, 2.0, 2.5, and 3.0-mg/mL particle concentrations was prepared and then separately mixed with various amounts of EVA shreds. When the solution became colloidal it was left at 30°C to 35°C under continuous stirring until uniform solutions were formed. (The viscosity information of as-prepared EVA/p-xylene solution is provided in Figure S1, Supporting Information). Finally, the mixture solution was screen-printed on the textured surface of the solar cells using a rotary roller (K Lox Proofer, RK PrintCoat Instruments, UK). The coated cells with wet films (coated surface area =  $5 \times 5$  cm) were dried in a fume hood and then cured in a furnace at 190°C for 5 minutes in order to obtain a glossy and thermal stable layer.<sup>32</sup> In addition, the solar cells with EVA/undoped- $Gd_2O_2S$  and solely EVA coatings (9, 12, 15, 18, and 21 wt%) were also produced for comparisons. The fabrication process of the EVA/ $Gd_2O_2S:Tb^{3+}$  modified mono-Si solar cell is illustrated in Figure 1.

## 2.4 | Characterization

The *J-V* characteristics of solar cells with and without EVA/phosphor coatings were analysed using a Trisol Class AAA xenon flash solar simulator (OAI Trisol TSS156, USA) under one-sun illumination ( $100 \text{ mW/cm}^2$ ) and room temperature conditions. The solar simulator can cover the spectrum from 350 to 1200 nm, as shown in Figure 2 (the spectral mismatch error was estimated to be less than 1%). During the measurement, the uncoated and coated part of each solar cell was masked by an artificially designed plate with a circular hole to determine an illuminated surface area of approximately  $8.553 \pm 0.027 \text{ cm}^2$ . Photocurrent-voltage characteristics was measured using a source metre (Keithley 2601B, USA). EQE measurements were performed using a monochromator-based solar cell response system (Bentham PVE300, UK). The reflectance and absorption spectra were recorded using a dual-beam ultraviolet-visible (UV-Vis) spectrophotometer (Perkin-Elmer Lambda 650S, USA). The refractive indices of the deposited layers were measured using a monochromatic ellipsometer (Rudolph Auto EL III, USA), equipped with a helium-neon-laser operating at 632.8 nm wavelength. (The refractive index accuracy is  $\pm 0.01$ ). Photoluminescence (PL) measurements were carried out by using a Bentham Instruments dual-monochromator system (Bentham M300, UK). Emission spectra were recorded from 300 to 800 nm with step size of 1 nm, while the excitation spectra were recorded by monitoring the dominant emission peak. International Commission on Illumination (CIE) colour coordinate was obtained from the spectra in terms of the 1931 CIE standard for

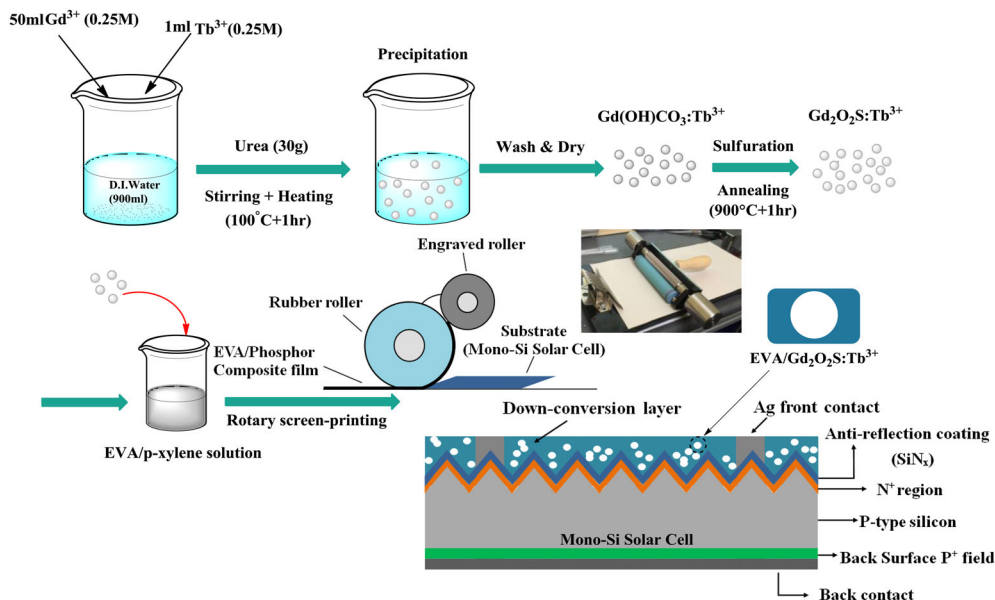


**FIGURE 1** Flow diagram showing the fabrication process of  $\text{Gd}_2\text{O}_2\text{S}:\text{Tb}^{3+}$  phosphor and the integration of composite material (EVA/ $\text{Gd}_2\text{O}_2\text{S}:\text{Tb}^{3+}$ ) on the textured surface of mono-Si solar cell [Colour figure can be viewed at [wileyonlinelibrary.com](http://wileyonlinelibrary.com)]

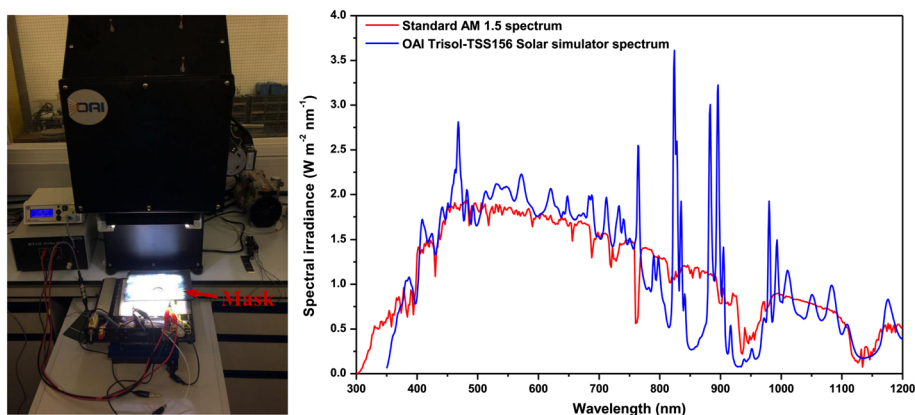


**FIGURE 2** Output spectrums of solar simulator and the standard AM 1.5 and a photograph showing the simulator [Colour figure can be viewed at [wileyonlinelibrary.com](http://wileyonlinelibrary.com)]

colorimetry. The quantum efficiency of the synthesized submicron phosphor was measured in a 60-mm integrating sphere accessory of a fluorescence spectrophotometer (Hitachi F-7000, Japan) by using its incorporated FL solution software based on the absolute method.<sup>33</sup>

The crystalline phases of the product was identified using a Bruker D8 Advance X-ray powder diffractometer (XRPD) with  $\text{CuK}\alpha$  ( $\lambda = 0.154 \text{ nm}$ ) radiation over the  $2\theta$  range from  $10^\circ$  to  $60^\circ$ . The diffractometer was previously calibrated using an aluminium oxide line position standard from Bruker and  $\text{LaB}_6$  NIST SRM 660a line profile standard. The experimental data were analysed using Bruker's TOPAS version III Rietveld refinement software.

The surface morphologies were obtained with a field emission scanning electron microscope (FESEM) (SUPRA 35VP, Zeiss, Germany). Energy dispersive X-ray spectroscopy (EDS) was used for elemental analysis of the deposited layers. The structural features and cathodoluminescence (CL) properties were examined using

a scanning transmission electron microscope (STEM) (JEM-2100F, JEOL, Japan). CL images were collected using a Gatan Vulcan system (Gatan Inc., USA).

## 3 | RESULTS AND DISCUSSION

### 3.1 | X-ray powder diffraction (XRPD)

Figure 3 presents the XRPD patterns of the as-synthesized  $\text{Gd}_2\text{O}_2\text{S}:\text{Tb}^{3+}$  and undoped- $\text{Gd}_2\text{O}_2\text{S}$  samples calcined at  $900^\circ\text{C}$ . The obtained result indicates that the fired particles show the characteristic XRPD pattern of the hexagonal  $\text{Gd}_2\text{O}_2\text{S}$  crystal, the representative diffraction peaks at  $13.29^\circ$  ( $13.27^\circ$ ),  $26.72^\circ$  ( $26.69^\circ$ ),  $29.95^\circ$  ( $29.89^\circ$ ),  $38.16^\circ$  ( $38.12^\circ$ ), and  $40.59^\circ$  ( $40.56^\circ$ ) for  $\text{Gd}_2\text{O}_2\text{S}:\text{Tb}^{3+}$  and undoped- $\text{Gd}_2\text{O}_2\text{S}$  can be indexed to the (001), (100), (101), (102), and (003)

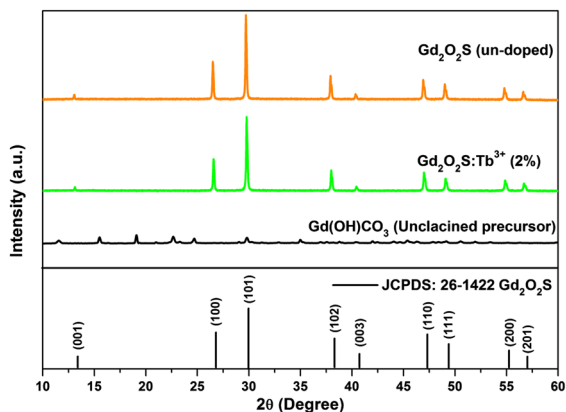


**FIGURE 3** X-ray powder diffraction (XRPD) patterns of  $\text{Gd}_2\text{O}_2\text{S}:\text{Tb}^{3+}$  and undoped- $\text{Gd}_2\text{O}_2\text{S}$  samples annealed at  $900^\circ\text{C}$  for 1 hour in air atmosphere [Colour figure can be viewed at [wileyonlinelibrary.com](#)]

plane of the hexagonal  $\text{Gd}_2\text{O}_2\text{S}$  phase, respectively, which are in good accordance with the standard JCPDS data file (No. 26–1422); no other detectable XRPD patterns were found, indicating that the resultant products are highly purified and that the doping ion ( $\text{Tb}^{3+}$ ) induces little variation in the  $\text{Gd}_2\text{O}_2\text{S}$  host crystal structure. The estimated crystallite sizes, hexagonal lattice parameters, and inter-planar spacing of the synthesized  $\text{Gd}_2\text{O}_2\text{S}$  samples are summarized in Table 1.

### 3.2 | Photoluminescence properties of synthesized phosphor particles

Figure 4 shows the PL and PL excitation (PLE) spectra of  $\text{Gd}_2\text{O}_2\text{S}:\text{Tb}^{3+}$  measured at room temperature. The excitation spectrum shows a wide absorption band from 250 to 334 nm, with a peak maximum at 292 nm. When the calcined  $\text{Gd}_2\text{O}_2\text{S}:\text{Tb}^{3+}$  phosphors were excited by 292 nm UV light, the emission bands at 488, 543, 585, and 622 nm were observed, respectively, in the PL spectrum. Among them, the green emission at 543 nm is the most intense band, with PL intensity reaching 39.1% in comparison with that of values for the sub-emission bands centred at 488 (9.2%), 585 (3.7%), and 622 nm (6.2%), respectively. This is assigned to the  $^5\text{D}_4 \rightarrow ^7\text{F}_5$  transitions of  $\text{Tb}^{3+}$  cations, as is revealed in the inset plot of Figure 4. This transition also proved for the intense green luminescence that can be seen by the naked eye under the irradiation of a UV lamp (see inset photograph in Figure 4). The colour coordinate for the  $\text{Tb}^{3+}$ -doped sample is  $x = 0.339$  and  $y = 0.586$ , which is located in the green region of the CIE 1931 chromaticity diagram, as shown in Figure 5. The result indicates that this phosphor can be a candidate as an adapted green phosphor for UV-blue lights.

**TABLE 1** The crystallite size and hexagonal lattice parameters of  $\text{Gd}_2\text{O}_2\text{S}:\text{Tb}^{3+}$  phosphor and  $\text{Gd}_2\text{O}_2\text{S}$  host particles from X-ray powder diffraction (XRPD) data

Sample	Crystallite Size (nm)	a (Å)	c (Å)	(hkl)	$d_{hkl}$ (Å)
$\text{Gd}_2\text{O}_2\text{S}:\text{Tb}^{3+}$	157.4	3.854	6.667	100	3.334
Undoped $\text{Gd}_2\text{O}_2\text{S}$	158.2	3.852	6.666	100	3.337

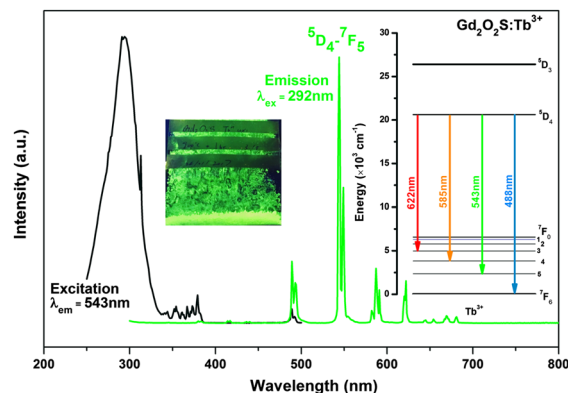


**FIGURE 4** Excitation ( $\lambda_{\text{em}} = 543$  nm) and emission ( $\lambda_{\text{ex}} = 292$  nm) spectra of  $\text{Gd}_2\text{O}_2\text{S}:\text{Tb}^{3+}$  particles calcined at  $900^\circ\text{C}$  for 1 hour. The inset shows the schematic energy level diagram of a free  $\text{Tb}^{3+}$  cation with proposed excitation and emission process, and a photograph of as-prepared phosphor sample showing bright green emission under irradiation with a 365 nm quartz tube lamp [Colour figure can be viewed at [wileyonlinelibrary.com](#)]

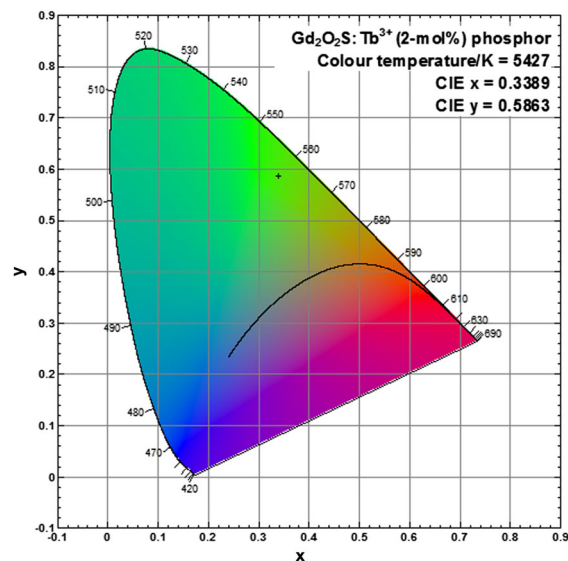


**FIGURE 5** International Commission on Illumination (CIE) chromaticity diagram showing the  $x$  and  $y$  coordinates of  $\text{Gd}_2\text{O}_2\text{S}:\text{Tb}^{3+}$  sample excited by 254 nm ultraviolet (UV) light [Colour figure can be viewed at [wileyonlinelibrary.com](#)]

To evaluate the performance and the emission efficiency of  $\text{Tb}^{3+}$ -doped phosphors for solar cell applications, the PL quantum yield (QY) measurements are performed. Table 2 summarizes the QY ( $\eta$ ) and energy absorption efficiency ( $\varphi$ ) of the synthesized  $\text{Gd}_2\text{O}_2\text{S}:\text{Tb}^{3+}$  at excitation wavelength of 254 and 292 nm, respectively. In present

**TABLE 2** Photoluminescence (PL) quantum yield and energy absorption efficiency of the  $\text{Gd}_2\text{O}_2\text{S:Tb}^{3+}$  phosphor sample

Sample ID	QY ( $\eta$ )	$\phi$
$\text{Gd}_2\text{O}_2\text{S:Tb}^{3+}$ (2 mol%)	%	%
Ex 254 nm	40.9	50.3
Ex 292 nm	47.3	57.2

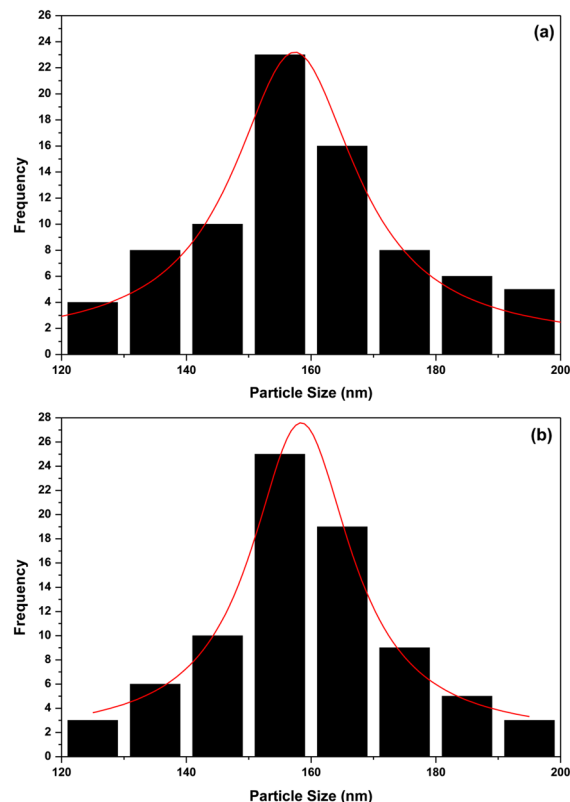
work, the QY ( $\eta$ ) and ( $\phi$ ) were measured with an integrating sphere by using the absolute method presented by De Mello et al.<sup>33</sup> Results indicate that under excitation wavelength at 292 nm, the measured QY ( $\eta$ ) and ( $\phi$ ) of the  $\text{Gd}_2\text{O}_2\text{S:Tb}^{3+}$  submicron hexagons show the highest values of 47.3% and 57.2%, respectively, which conforms to the required luminescent down-converter QY value of 40% to improve the energy performance of solar cell devices.<sup>34</sup>

These results also suggest that the as-prepared,  $\text{Gd}_2\text{O}_2\text{S:Tb}^{3+}$  phosphor possesses the down-converting properties by absorbing and converting high-energy UV photons into the visible spectrum, which could potentially contribute to enhanced photocurrent production, thus raising the conversion efficiency of mono-Si solar cells.

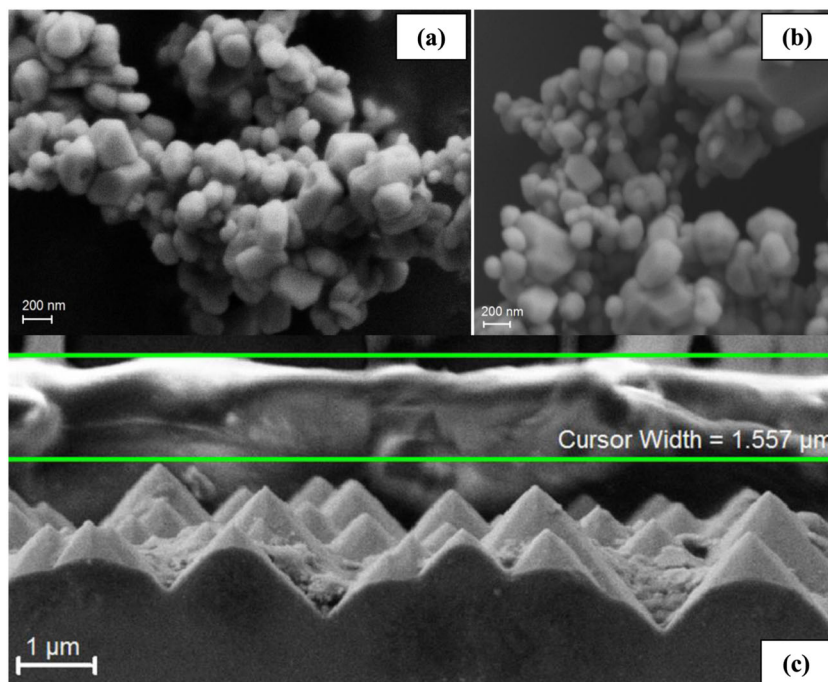
### 3.3 | Morphology and structure analysis

Figure 6A and 6B show the typical FE-SEM micrographs of synthesized  $\text{Gd}_2\text{O}_2\text{S:Tb}^{3+}$  and undoped- $\text{Gd}_2\text{O}_2\text{S}$  particles. It can be seen that they exhibit smooth and well-formed crystals, although there is some agglomeration. Most of the particles have truncated spherical-like shape. The corresponding average particle size obtained from Lorentzian fitting of FE-SEM observations is 160.3 nm for  $\text{Gd}_2\text{O}_2\text{S:Tb}^{3+}$  and 161.1 nm for undoped- $\text{Gd}_2\text{O}_2\text{S}$  (with

determination coefficient  $R^2$  values of 0.911 and 0.971, respectively), as demonstrated in the histograms presented in Figure 7. These results are consistent with the calculated data from the XRPD



**FIGURE 7** Histogram of (A)  $\text{Gd}_2\text{O}_2\text{S:Tb}^{3+}$  and (B) undoped  $\text{Gd}_2\text{O}_2\text{S}$  submicron phosphor samples showing Lorentzian curve fit in red [Colour figure can be viewed at wileyonlinelibrary.com]



**FIGURE 6** Field emission-scanning electron microscope (FE-SEM) micrographs of (A) representative  $\text{Gd}_2\text{O}_2\text{S:Tb}^{3+}$  and (B) undoped- $\text{Gd}_2\text{O}_2\text{S}$  particles annealed at  $900^\circ\text{C}$ ; (C) cross section image of the mono-Si solar cell after coating with EVA/ $\text{Gd}_2\text{O}_2\text{S:Tb}^{3+}$ , the integration of phosphor particles on the cell's textured surface is observed [Colour figure can be viewed at wileyonlinelibrary.com]

measurements (see Table 1). Figure 6C displays the cross section image of a mono-Si cell after coating with EVA/Gd<sub>2</sub>O<sub>2</sub>S:Tb<sup>3+</sup> (2.0-mg/mL particle density). It shows clearly the morphology of pyramidally textured silicon surface and the coated luminescent layer composed of EVA/Gd<sub>2</sub>O<sub>2</sub>S:Tb<sup>3+</sup>, with an average thickness of 1.56 μm. (The variation of film thickness due to the change of EVA wt% are illustrated in Figure S2 and S3, Supporting Information). In addition, we have observed that some of the Gd<sub>2</sub>O<sub>2</sub>S:Tb<sup>3+</sup> particles are deposited onto the cell's surface through rotary screen printing, and most of the particles are well-encapsulated by the EVA binder. The EDS (see Figure 8) from the cross-sectional scanning area of coated cells confirms that the deposited layers contain gadolinium (Gd), oxygen (O), sulfur (S), and terbium (Tb) elements. The additional intense peak in regarding to carbon (C) is from the EVA binder.

Figure 9 shows the high angle annular dark field (HAADF) STEM images of the Gd<sub>2</sub>O<sub>2</sub>S:Tb<sup>3+</sup> particles fabricated in this work. In Figure 9A, the discrete particles of roughly hexagonal shape with apparently a smooth surface can be clearly observed. In Figure 9B, the light distribution image of a small cluster is seen, and the distribution of light appearing from part of the crystals is fairly uniform, where some areas are brighter. The overlay image (see Figure 9C) shows the high uniformity of visible light (green) emission from the submicron sized phosphor particles.

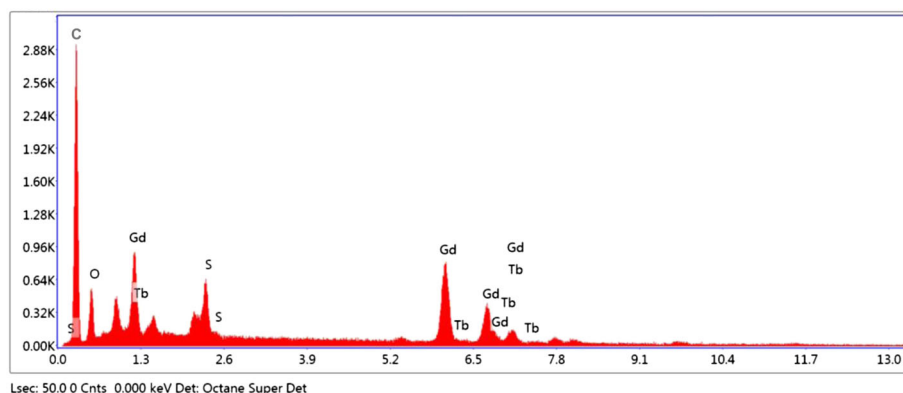


**FIGURE 8** Energy dispersive X-ray spectroscopy (EDS) of mono-Si solar cell coated with EVA/Gd<sub>2</sub>O<sub>2</sub>S:Tb<sup>3+</sup> [Colour figure can be viewed at [wileyonlinelibrary.com](http://wileyonlinelibrary.com)]

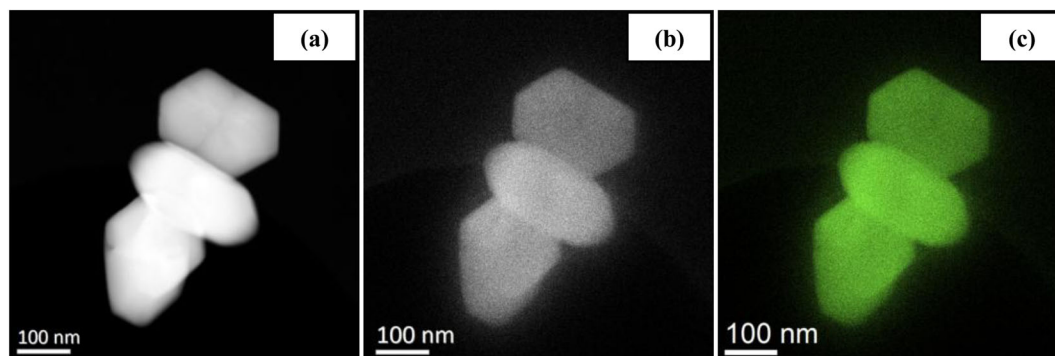


**FIGURE 9** Scanning transmission electron microscope (STEM) micrographs of (A) single crystals of Gd<sub>2</sub>O<sub>2</sub>S:Tb<sup>3+</sup>; (B) total visible light (CL) image using the VULCAN detector; (C) overlay of images of (A) and (B) [Colour figure can be viewed at [wileyonlinelibrary.com](http://wileyonlinelibrary.com)]

### 3.4 | Electrical characteristics of coated solar cell

Figure 10 presents and compares the *J*-*V* curves of bare, solely EVA (15-wt%) binder-coated, EVA/Gd<sub>2</sub>O<sub>2</sub>S:Tb<sup>3+</sup> (2.0-mg/mL)-coated, and EVA/undoped-Gd<sub>2</sub>O<sub>2</sub>S (2.0-mg/mL)-coated solar cells. The corresponding electrical characteristics that were obtained are summarized in Table 4. The bare mono-Si solar cell exhibited a power conversion efficiency (PCE) of 16.43%, a short-circuit current density (*J*<sub>sc</sub>) of 37.85 mA/cm<sup>2</sup> and an open-circuit voltage (*V*<sub>oc</sub>) of 604.6 mV. By comparing the effects of various weight ratios of EVA coatings on the *J*-*V* characteristics of the bare solar cells, we found that coated cell with solely EVA at 15 wt% ratio showed negligible changes in *V*<sub>oc</sub> (603.5 mV) and *J*<sub>sc</sub> (37.82 mA/cm<sup>2</sup>), giving rise to a marginal decrease of 0.07% (from 16.43% to 16.36%) in PCE. This ratio of coating provides the best electrical performance compared with other ratios of pure EVA coatings (see Table 3), which potentially contributed to maximizing the PCE enhancement. As indicated, the EVA serves as binder for the Gd<sub>2</sub>O<sub>2</sub>S:Tb<sup>3+</sup> particles and these layers tend to slightly reduce the solar cell's efficiency. In this case, it is pivotal to find a certain wt% of EVA that decreases efficiency by the smallest amount. The highest increase in *J*<sub>sc</sub> and *V*<sub>oc</sub>, corresponding to a maximum enhancement of 3.6% (from 16.43% to 17.02%) in PCE compared with that of bare cell, was achieved by applying EVA/Gd<sub>2</sub>O<sub>2</sub>S:Tb<sup>3+</sup> (2.0-mg/mL particle

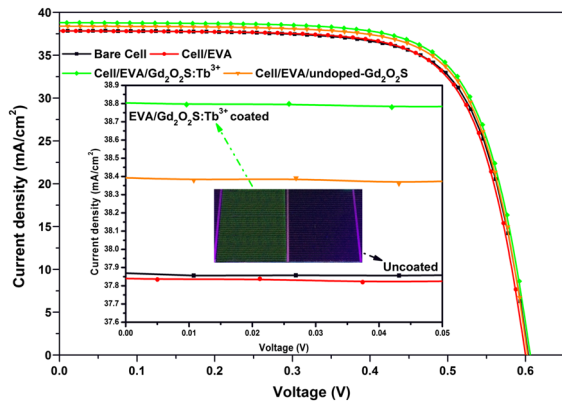


**FIGURE 10** *J*-*V* curves of mono-Si solar cells with the following configurations: A bare cell, a cell coated with solely EVA (15 wt%) binder, a cell coated with EVA/undoped-Gd<sub>2</sub>O<sub>2</sub>S (2.0 mg/mL), and a cell coated with EVA/Gd<sub>2</sub>O<sub>2</sub>S:Tb<sup>3+</sup> (2.0 mg/mL). Inset shows a digital photograph of solar cell coated with EVA/Gd<sub>2</sub>O<sub>2</sub>S:Tb<sup>3+</sup> (2.0 mg/mL) composite layer irradiated by ultraviolet (UV) light [Colour figure can be viewed at [wileyonlinelibrary.com](http://wileyonlinelibrary.com)]

**TABLE 3** Power conversion efficiency (PCE) change in mono-Si solar cell with different wt% ratios of ethylene vinyl acetate (EVA)

Cell Type	Ratio-In wt%	Uncoated $\eta$ (%)	Coated $\eta$ (%)	Variation in $\eta$ (%)
EVA	9	16.45	16.24	-0.21
EVA	12	16.38	16.25	-0.13
EVA	15	16.43	16.36	-0.07
EVA	18	16.40	16.30	-0.10
EVA	21	16.44	16.28	-0.16

density) on the cell's textured surface. This coating led to a relative increase of 2.5% in  $J_{sc}$  (from 37.85 to 38.81 mA/cm<sup>2</sup>), which is most likely the factor that contributed to the enhancement in PCE. In comparison, the enhancement brought by the EVA/undoped Gd<sub>2</sub>O<sub>2</sub>S coating at same particle density is less obvious, with  $J_{sc}$  increased by 1.5% (from 37.85 to 38.40 mA/cm<sup>2</sup>), corresponding to an overall increase of 2.3% (from 16.43% to 16.80%) in conversion efficiency. This phenomenon is due to the absence of doping agent (Tb<sup>3+</sup>), and thus, the lack of certain UV photons for subsequent DC process. In such case, the improved light absorption is solely expected to benefit from the light scattering of the host particles, which is discussed in more details in Section 3.5.

In addition, we have also observed that the enhancement contributed from both dispersed phosphor and host particles at different concentrations in EVA binder can be achieved (see Table 4 and Figure 11). As illustrated in Figure 11, in both cases, the enhancement coefficient started to drop when the particle density exceeded 2.0 mg/mL; and eventually, the conversion efficiency began to deteriorate when the particle concentrations were higher than around 2.7 mg/mL. The reduction in PCE at 3.0 mg/mL particle density may have been caused by the significant backward scattering arising from the serious particle aggregation. At higher

**TABLE 4** *J*-*V* characteristics of all evaluated solar cells

Type	$J_{sc}$ (mA/cm <sup>2</sup> )	$V_{oc}$ (mV)	$P_{max}$ (W)	FF (%)	PCE (%)
Uncoated	37.85	604.6	0.1405	71.81	16.43
Cell/EVA	37.82	603.5	0.1399	71.71	16.36
Cell/EVA/Gd <sub>2</sub> O <sub>2</sub> S:Tb <sup>3+</sup> (1.0 mg/mL)	38.04	605.3	0.1415	71.88	16.54
Cell/EVA/Gd <sub>2</sub> O <sub>2</sub> S:Tb <sup>3+</sup> (1.5 mg/mL)	38.40	606.9	0.1440	72.19	16.83
Cell/EVA/Gd <sub>2</sub> O <sub>2</sub> S:Tb <sup>3+</sup> (2.0 mg/mL)	38.81	608.0	0.1456	72.15	17.02
Cell/EVA/Gd <sub>2</sub> O <sub>2</sub> S:Tb <sup>3+</sup> (2.5 mg/mL)	38.42	605.8	0.1430	71.90	16.72
Cell/EVA/Gd <sub>2</sub> O <sub>2</sub> S:Tb <sup>3+</sup> (3.0 mg/mL)	37.56	598.5	0.1377	71.60	16.10
Cell/EVA/Gd <sub>2</sub> O <sub>2</sub> S (1.0 mg/mL)	37.90	604.6	0.1407	71.83	16.45
Cell/EVA/Gd <sub>2</sub> O <sub>2</sub> S (1.5 mg/mL)	38.19	605.6	0.1421	71.86	16.61
Cell/EVA/Gd <sub>2</sub> O <sub>2</sub> S (2.0 mg/mL)	38.40	606.4	0.1437	72.12	16.80
Cell/EVA/Gd <sub>2</sub> O <sub>2</sub> S (2.5 mg/mL)	38.12	604.9	0.1417	71.83	16.57
Cell/EVA/Gd <sub>2</sub> O <sub>2</sub> S (3.0 mg/mL)	37.50	598.7	0.1374	71.63	16.06

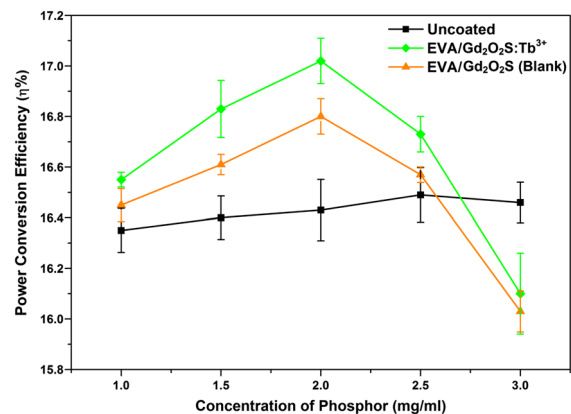


**FIGURE 11** Enhancement in PCE of mono-Si solar cells coated with different concentrations of Gd<sub>2</sub>O<sub>2</sub>S:Tb<sup>3+</sup> and Gd<sub>2</sub>O<sub>2</sub>S (blank) materials [Colour figure can be viewed at [wileyonlinelibrary.com](http://wileyonlinelibrary.com)]

concentration, the substantial absorption in the UV region by Gd<sub>2</sub>O<sub>2</sub>S:Tb<sup>3+</sup> phosphors that induced thicker phosphor films on the solar cell surfaces, which undermines the original light-trapping capability from the solar cell's intrinsic textured surface and this will become more apparent with the increasing of particles density whether they are doped or undoped. As a result, it creates shading on the pyramid textured surface that affected significantly the original transmittance towards the cell in both UV and visible region, which in turn overshadowed the DC effects.



### 3.5 | Optical characteristics of coated solar cell

To further validate the obtained results regarding the efficiency enhancement brought by the  $\text{Gd}_2\text{O}_2\text{S}:\text{Tb}^{3+}$  phosphor particles, we performed reflectance measurements. Figure 12 shows the reflectance and absorption spectra for bare cell, solely EVA (15 wt%) binder-coated, EVA/ $\text{Gd}_2\text{O}_2\text{S}:\text{Tb}^{3+}$  (2.0 mg/mL) and EVA/undoped- $\text{Gd}_2\text{O}_2\text{S}$  (2.0 mg/mL)-coated solar cells. Comparing with the bare solar cell, the coated cell with EVA/ $\text{Gd}_2\text{O}_2\text{S}:\text{Tb}^{3+}$  exhibits overall reduction in reflectance across the measured spectral wavelength range of 200 to 850 nm (see Figure 12A). This can be explained based on the two optical features. In the range of wavelength below 400 nm, the reflectance dropped because of the absorption of UV photons by  $\text{Gd}_2\text{O}_2\text{S}:\text{Tb}^{3+}$  phosphor particles. The drastic reduction, particularly in the UV-region of 290 to 380 nm by absorbing high-energy incident photons eventually achieved an overall reduction by almost 20% compared with that of a bare cell. On the other hand, as shown in Figure 12B, where in the range of wavelength above 400 nm, the absorption spectrum shows obvious increase in light absorption in the spectral range from 500 to 850 nm, since there is no PLE signal presented in the excitation spectrum (see Figure 4), therefore, we consider that the improved light absorption is associated with the light scattering from the phosphor particles. Similarly, in the case of EVA/undoped- $\text{Gd}_2\text{O}_2\text{S}$  coated cell, analogous levels of light absorption in the visible region can be also

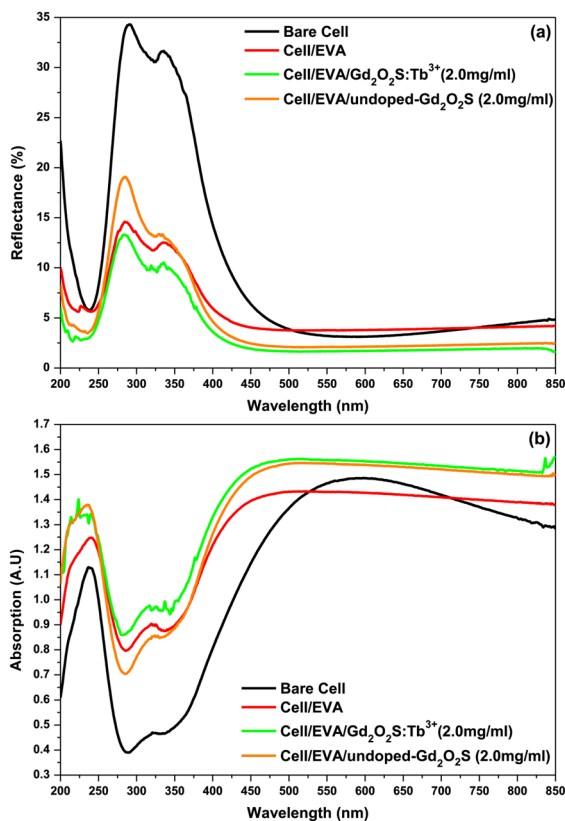


**FIGURE 12** Optical (A) reflectance and (B) absorbance of uncoated and coated cells [Colour figure can be viewed at [wileyonlinelibrary.com](http://wileyonlinelibrary.com)]

observed. This is most likely because of the light scattering provided from the hexagonal  $\text{Gd}_2\text{O}_2\text{S}$  particles, which is believed to be essential for partially trapping and coupling of normally incident photons into the solar cell's active layers.<sup>34,35</sup> However, the higher value of reflectance at UV-blue wavelengths compared with that of EVA/ $\text{Gd}_2\text{O}_2\text{S}:\text{Tb}^{3+}$ -coated device is ascribed to lacking functional features of UV absorbing ability without the presence of Tb-doping agent in the host crystal. Furthermore, the comparison also demonstrates that the reflectance at wavelengths of 200 to 500 nm can be reduced when the cell's surface is coated with pure EVA, which approximately achieves good agreement with the relevant results with regard to the EVA's optical properties reported in literature<sup>36</sup> and our predictions since the average refractive index (RI) of EVA ( $n \approx 1.48\text{--}1.49$ ) in use at present is between the  $\text{SiN}_x$  ( $n \approx 1.9$ ) and air ( $n \approx 1$ ).<sup>37,38</sup> It is noteworthy that a matrix with a proper RI value is conducive, thus minimizing the Fresnel Reflection Loss during the light absorption at the interface. To obtain the minimum reflection in a single-layer of anti-reflection coating (ARC), the refractive index of a typical antireflective material is desired to be equal to the square root of refractive indices of the materials bounding the coating.<sup>39</sup> As in our case, the deposited composite layer of EVA/ $\text{Gd}_2\text{O}_2\text{S}:\text{Tb}^{3+}$ , EVA/undoped- $\text{Gd}_2\text{O}_2\text{S}$ , and solely EVA film show average RI of  $n = 1.593$ ,  $n = 1.561$ , and  $n = 1.482$ , respectively; in each case, the coated layer is able to provide improved RI matching when sandwiched between the  $\text{SiN}_x$  layer and air, which can be potentially served as an alternative anti-reflection coating.<sup>16</sup> Unexpectedly, we observed that the solely EVA (15 wt%) coating exhibits good light transparency with transmittance close to that of a quartz substrate ( $T(\lambda)_{\text{EVA}}$  versus  $T(\lambda)_{\text{quartz}} = 93.1/93.5$  over the range from 250 to 400 nm and  $91.8/92.6$  in the range of 400 to 850 nm) (see Figure 13). This is of crucial importance since the binding material must possess relatively high transmittance or even provide minor anti-reflective probabilities that would not offset the potential enhancement originated by the phosphor particles. (More information in regard to the optical reflectance and transmission

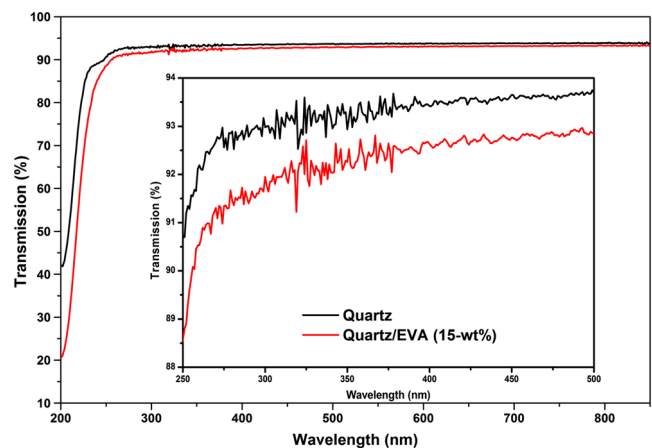


**FIGURE 13** Transmission spectra for quartz substrate and the deposited film with 15 wt% solely ethylene vinyl acetate (EVA) coating [Colour figure can be viewed at [wileyonlinelibrary.com](http://wileyonlinelibrary.com)]

properties of all evaluated solely EVA coatings are presented and compared in Figure S4, Supporting Information).

### 3.6 | External quantum efficiency (EQE) characterization

External quantum efficiency measurements were performed to clarify the underlying mechanisms for the enhanced solar cell efficiency. The recorded EQE spectra are shown in Figure 14. The EQE value for binder-coated cells is fairly close to that of bare cells and is slightly higher at wavelengths of 300 to 380 nm, which coincides with the obtained reflectance results (see Figure 12A). Moreover, the solar cell coated with the EVA/Gd<sub>2</sub>O<sub>2</sub>S:Tb<sup>3+</sup> composite layer shows overall higher EQE value than the bare cell across the entire wavelengths range of 300 to 1100 nm, and a maximum relative enhancement over 19% in the UV regions was observed, indicating explicitly that the increase in photocurrent is mostly arisen from the enhanced absorption of UV photons by the Gd<sub>2</sub>O<sub>2</sub>S:Tb<sup>3+</sup> phosphors. Since a large proportion of electron-hole pairs derived from absorbing high energy photons usually situated near the solar cell surface, the photo-generated carriers subsequently consume and disappear easily through their recombination because of the surface defects, which

may in turn give rise to inferior carrier collection possibilities.<sup>16,17</sup> Nevertheless, with the presence of the phosphor particles on the front surface of mono-Si solar cell, a greater number of photons can be absorbed closer to the depletion region for photo-current generation as soon as the UV photons are luminescent converted to the visible region of solar spectrum. With the effect of the internal electric field (E-field), the photo-generated electron-hole pairs will be instantaneously separated, and thus the enhancement in PV effect. As for the enhanced EQE response above 400 nm, the observed increase of EQE for both undoped-Gd<sub>2</sub>O<sub>2</sub>S and Gd<sub>2</sub>O<sub>2</sub>S:Tb<sup>3+</sup> cases are in consistent with the variation of corresponding reflectance spectra, as illustrated in Figure 12A. We consider that this enhanced behaviour was mainly attributed to the improved light trapping on the basis of scattering by the submicrometer Gd<sub>2</sub>O<sub>2</sub>S hexagons. However, the reduced EQE value for EVA/undoped-Gd<sub>2</sub>O<sub>2</sub>S, in comparison with that of EVA/Gd<sub>2</sub>O<sub>2</sub>S:Tb<sup>3+</sup> particularly near the UV region (300 to 420 nm), proves that the doping ions (Tb<sup>3+</sup>) is solely responsible for the absorption of UV photons and later on the DC process for further photocurrent generation of mono-Si solar cells. These results also demonstrate that the integration of Gd<sub>2</sub>O<sub>2</sub>S:Tb<sup>3+</sup> phosphor particles on the textured surface of mono-Si solar cells are able to increase the EQE within UV-region via DC effects and at longer wavelength through light scattering. In addition, most importantly, the EVA binder used to encapsulate the phosphor particles to the solar cell exhibits excellent visible light transmittance, and also good light absorption particularly at short-wavelengths of UV-region (see Figure 12B and Figure 13), which did not disrupt the original DC functionality and uniform-light-scattering effect of the phosphor particles. Figure 14B plots the enhancement factor for coated cells with maximum enhancement in EQE, relative to those for a bare cell. The cells coated with EVA/Gd<sub>2</sub>O<sub>2</sub>S:Tb<sup>3+</sup> (2.0 mg/mL) achieved the maximal EQE enhancement factor (more than 1.15 at 300-400 nm and more than 1.03 at 400-1100 nm), followed by the cells coated with EVA/undoped-Gd<sub>2</sub>O<sub>2</sub>S (2.0 mg/mL) (more than 1 at 410-1100 nm), and then by cell coated with solely EVA (15 wt%) binder (more than 1 at 300-400 nm).

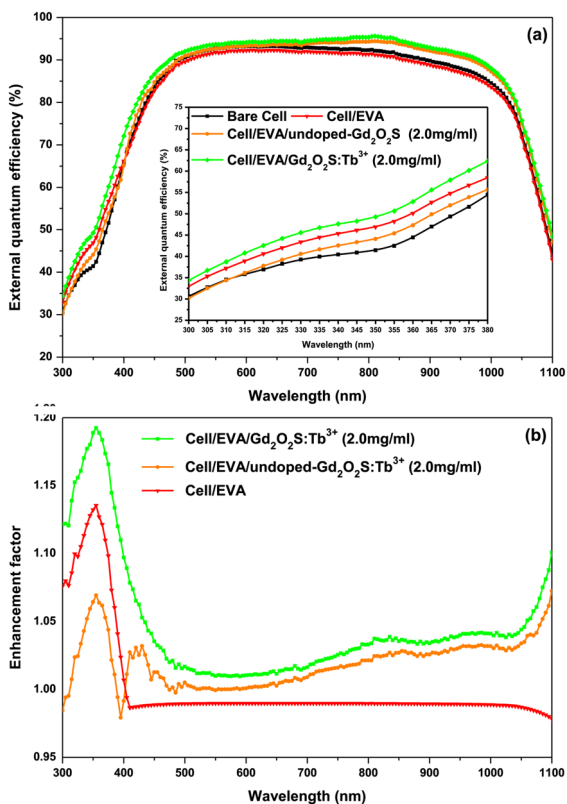


**FIGURE 14** (A) External quantum efficiency (EQE) curves at maximum enhancement for solar cells integrated with Gd<sub>2</sub>O<sub>2</sub>S submicron phosphors; (B) enhancement factor of EQE for solar cells coated with solely ethylene vinyl acetate (EVA), EVA/Gd<sub>2</sub>O<sub>2</sub>S:Tb<sup>3+</sup>, and EVA/undoped-Gd<sub>2</sub>O<sub>2</sub>S, compared with that of bare cell [Colour figure can be viewed at [wileyonlinelibrary.com](http://wileyonlinelibrary.com)]

## 4 | CONCLUSIONS

In this work, we developed a simple and cost-effective luminescent layer applied onto the textured surface of mono-Si solar cells and demonstrated that the down-converting Gd<sub>2</sub>O<sub>2</sub>S:Tb<sup>3+</sup> phosphor could effectively improve the conversion efficiency of the cell. The empirical results showed an optimum enhancement of 3.6% (from 16.43% to 17.02%) in PCE, relative to those for a pristine cell. This enhancement was attributed to the improved light absorption brought by the conjunction effects of EVA binder and Gd<sub>2</sub>O<sub>2</sub>S:Tb<sup>3+</sup> phosphor. The integration of Tb-doped phosphor particles on a front-textured solar cell can enhance the EQE within the UV-region through DC effects and within the visible-region through forward light scattering. Gd<sub>2</sub>O<sub>2</sub>S:Tb<sup>3+</sup> submicron phosphor, as the down-converting material with a high quantum efficiency (approximately 47%), is a suitable alternative to obtain an enhanced solar cell performance at a relatively low cost

and is environmentally friendly. An EVA matrix provides promising host conditions for the phosphor particles. Finally, the rotary screen printing formed a relatively uniform layer and we believe that it can be applied to various types of photovoltaic devices and other phosphor powders.

## ACKNOWLEDGEMENTS

The authors wish to thank Dr Ashley Howkins of the Experimental Techniques Centre for SEM/STEM analyses. We are grateful to Prof Jack Silver of the Centre for Phosphor and Display Materials for valuable discussions. We also express here our gratitude to Dr Shashi Paul and Mr Krishna Nama Manjunatha from De Montfort University, UK for the processing of the ellipsometric measurements.

## DECLARATIONS OF INTERESTS

None.

## ORCID

Fanchao Meng  <https://orcid.org/0000-0003-1338-8035>

## REFERENCES

- Battaglia C, Cuevas A, Wolf SD. High-efficiency crystalline silicon solar cell: status and perspectives. *Energ Environ Sci*. 2016;9(5):1552-1576.
- Green MA, Hishikawa Y, Dunlop ED, Levi DH, Hohl-Ebinger J, Ho-Bailie AWY. Solar cell efficiency tables (version 51). *Prog Photovolt Res Appl*. 2017;26(1):3-12.
- Green MA. *Third Generation Photovoltaic: Advanced Solar Energy Conversion*. Berlin & Heidelberg, Germany: Springer; 2003.
- Taube WR, Kumar A, Saravanan R, et al. Efficiency enhancement of silicon solar cell with silicon nanocrystals embedded in PECVD silicon nitride matrix. *Sol Energy Mater Sol Cells*. 2012;101:32-35.
- Shockley W, Queisser HJ. Detailed balance limit of efficiency of *p-n* junction solar cells. *J Appl Phys*. 1961;32(3):510-519.
- Chen YC, Huang WY, Chen TM. Enhancing the performance of photovoltaic cells by using down-converting KCaGd(PO<sub>4</sub>)<sub>2</sub>:Eu<sup>2+</sup> phosphors. *J Rare Earths*. 2011;29(9):907-910.
- Shehata N, Clavel M, Meehan K, Samir E, Gaballah S, Salah M. Enhanced erbium-doped ceria nanostructure coating to improve solar cell performance. *Materials*. 2015;8(11):7663-7672.
- Tahhan A, Dehouche Z, Fern GR, Haverkamp E. Photovoltaic cells energy performance enhancement with down-converting photoluminescence phosphors. *Int J Energy Res*. 2015;39(12):1616-1622.
- Wu XJ, Meng FZ, Zhang ZZ, Yu YN, Liu XJ, Meng J. Broadband down-conversion for silicon solar cell by ZnSe/phosphor heterostructure. *Opt Express*. 2014;22(S3):A735-A741.
- Richards BS. Luminescent layers for enhanced silicon solar cell performance: down-conversion. *Sol Energy Mater Sol Cells*. 2006;90(9):1189-1207.
- Trupke T, Green MA, Wüfel P. Improving solar cell efficiencies by down-conversion of high-energy photons. *J Appl Phys*. 2002;92(3):1668-1674.
- Chen JY, Huang CK, Hung WB, Sun KW, Chen TM. Efficiency improvement of Si solar cells using metal-enhanced nanophosphor fluorescence. *Sol Energy Mater Sol Cells*. 2014;120:168-174.
- Ho WJ, Deng YJ, Liu JJ, Feng SK, Lin JC. Photovoltaic performance characterization of textured silicon solar cells using luminescent down-shifting Eu-doped phosphor particles of various dimensions. *Materials*. 2017;10(1):21.
- Ho WJ, Shen YT, Liu JJ, You BJ, Ho CH. Enhancing photovoltaic performance using broadband luminescent down-shifting by combining multiple species of Eu-doped silicate phosphors. *Nanomaterials*. 2017;7(10):340.
- Ho WJ, Yang GC, Shen YT, Deng YJ. Improving efficiency of silicon solar cells using europium-doped silicate-phosphor layer by spin-on film coating. *Appl Surf Sci*. 2016;365:120-124.
- Huang CK, Chen YC, Hung WB, Chen TM, Sun KW, Chang WL. Enhanced light harvesting of Si solar cells via luminescent down-shifting using YVO<sub>4</sub>:Bi<sup>3+</sup>, Eu<sup>3+</sup> nanophosphors. *Prog Photovolt Res Appl*. 2013;21(7):1507-1513.
- Hung WB, Chen TM. Efficiency enhancement of silicon solar cells through a downshifting and antireflective oxysulfide phosphor layer. *Sol Energy Mater Sol Cells*. 2015;133:39-47.
- Liu J, Wang K, Zheng W, Huang W, Li CH, You XZ. Improving spectral response of monocrystalline silicon photovoltaic modules using high efficient luminescent down-shifting Eu<sup>3+</sup> complexes. *Prog Photovolt Res Appl*. 2013;21(4):668-675.
- Shao GJ, Lou CG, Xiao D. Enhancing the efficiency of solar cells by down shifting YAG:Ce<sup>3+</sup> phosphor. *JOL*. 2015;157:344-348.
- Jiang Y, Wu Y, Xie Y, Qian YT. Synthesis and characterization of nanocrystalline lanthanide oxysulfide via a La(OH)<sub>3</sub> gel solvothermal route. *J Am Ceram Soc*. 2004;83(10):2628-2630.
- Jiang GC, Wei XT, Zhou SS, Chen YH, Duan CK, Yin M. Neodymium doped lanthanum oxysulfide as optical temperature sensors. *JOL*. 2014;152:156-159.
- Zhao F, Yuan M, Zhang W, Gao S. Monodisperse lanthanide oxysulfide nanocrystals. *J Am Chem Soc*. 2006;128(36):11758-11759.
- Yoshida M, Nakagawa M, Fujii H, et al. Application of Gd<sub>2</sub>O<sub>2</sub>S ceramic scintillator for X-ray solid state detector in X-ray CT. *Jpn J Appl Phys*. 1988;27(8):L1572-L1575.
- Brüninghoff R, Engels DD, Fern GR, Ireland TG, Dhillon R, Silver J. Nanosized (Y<sub>1-x</sub>Gd<sub>x</sub>)<sub>2</sub>O<sub>2</sub>S:Tb<sup>3+</sup> particles: synthesis, photoluminescence, cathodoluminescence studies and a model for energy transfer in establishing the roles of Tb<sup>3+</sup> and Gd<sup>3+</sup>. *RSC Adv*. 2016;6(48):42561-42571.
- Mckenna B, Evans RC. Towards efficient spectral converters through materials design for luminescent solar devices. *Adv Mater*. 2017;29(28):1606491.
- Yan X, Fern GR, Withnall R, Silver J. Effects of the host lattice and doping concentration on the colour Tb<sup>3+</sup> cation emission in Y<sub>2</sub>O<sub>2</sub>S:Tb<sup>3+</sup> and Gd<sub>2</sub>O<sub>2</sub>S:Tb<sup>3+</sup> nanometer sized phosphor particles. *Nanoscale*. 2013;5(18):8640-8646.
- Fern GR, Ireland TG, Silver J, et al. Characterisation of Gd<sub>2</sub>O<sub>2</sub>S:Pr phosphor screens for water window X-ray detection. *Nucl Instrum Methods A*. 2009;600(2):434-439.
- Jing X, Ireland TG, Gibbons C, et al. Control of Y<sub>2</sub>O<sub>3</sub>:Eu spherical particle phosphor size, assembly properties, and performance for FED and HDTV. *J Electrochem Soc*. 1999;146(12):4654-4658.
- Silver J, Withnall R, Marsh PJ, Lipman A, Ireland TG, Fern GR. P-80: a new oxide/oxysulfide based phosphor triad and high-efficiency green-emitting (Y,Gd)<sub>2</sub>O<sub>2</sub>S:Tb phosphor for FED applications. *SID Int Symp Dig Tech*. 2005;36(1):594-597.
- Yuwawech K, Wootthikanokkhan J, Tanpichai S. Enhancement of thermal, mechanical and barrier properties of EVA solar cell encapsulating films by reinforcing with esterified cellulose nanofibres. *Polym Test*. 2015;48:12-22.

31. Yan X, Fern GR, Withnall R, Silver J. Contrasting behaviour of the co-activators in the luminescence spectra of  $Y_2O_3:S:Tb^{3+}$ ,  $Er^{3+}$  nanometer sized particles under UV and red light excitation. *Nanoscale*. 2013;5(3): 1091-1096.
32. Meng FC, Dehouche Z, Nutasarin A, Fern GR. Effective MgO-doped  $TiO_2$  nanoaerogel coating for crystalline silicon solar cells improvement. *Int J Energy Res*. 2018;42(12):3915-3927.
33. De Mello JC, Wittmann HF, Friend RH. An improved experimental determination of external photoluminescence quantum efficiency. *Adv Mater*. 1997;9(3):230-232.
34. Pi XD, Li Q, Li DS, Yang D. Spin-coating silicon-quantum-dot ink to improve solar cell efficiency. *Sol Energy Mater Sol Cells*. 2011;95(10): 2941-2945.
35. Hore S, Vetter C, Kern R, Smit H, Hirsch. Influence of scattering layers on efficiency of dye-sensitized solar cells. *Sol Energy Mater Sol Cells*. 2006;90(9):1176-1188.
36. Nagel H, Aberle AG, Hezel R. Optimised antireflection coatings for planar silicon solar cells using remote PECVD silicon nitride and porous silicon dioxide. *Prog Photovolt Res Appl*. 1999;7(4):245-260.
37. French RH, Rodríguez-Parada JM, Yang MK, Derryberry RA, Pfeifferberger NT. Optical properties of polymeric materials for concentrator photovoltaic systems. *Sol Energy Mater Sol Cells*. 2011;95(8):2077-2086.
38. Wei MC, Chang SJ, Tsia CY, Liu CH, Chen SC.  $SiN_x$  deposited by in-line PECVD for multi-crystalline silicon solar cells. *Sol Energy*. 2006;80(2): 215-219.
39. Macleod HA. *Thin-Film Optical Filters*. Bristol: Adam Hilger Ltd; 1986.

## SUPPORTING INFORMATION

Additional supporting information may be found online in the Supporting Information section at the end of the article.

**How to cite this article:** Meng F, Dehouche Z, Ireland TG, Fern GR. Improved photovoltaic performance of monocrystalline silicon solar cell through luminescent down-converting  $Gd_2O_3:S:Tb^{3+}$  phosphor. *Prog Photovolt Res Appl*. 2019;27:640-651. <https://doi.org/10.1002/pip.3139>